Inorganic Chemistry

including bioinorganic chemistry

July 7, 2014
Volume 53, Number 13
pubs.acs.org/IC

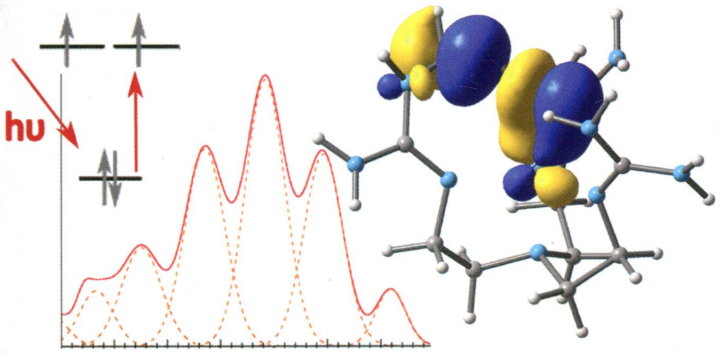

Forum on

Insights into Spectroscopy and Reactivity from Electronic Structure Theory

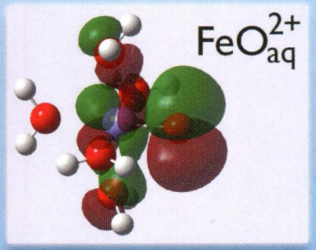

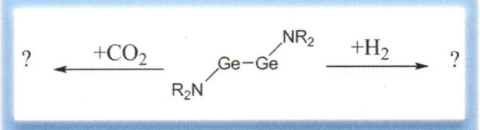

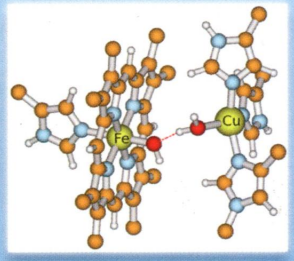

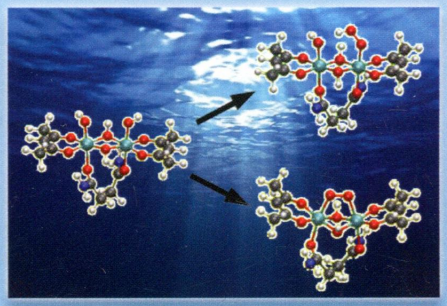

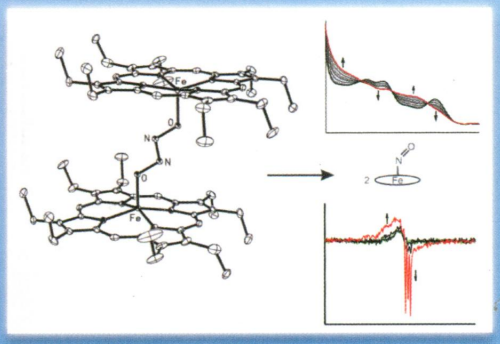

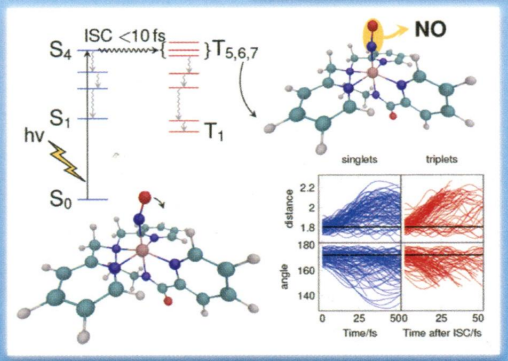

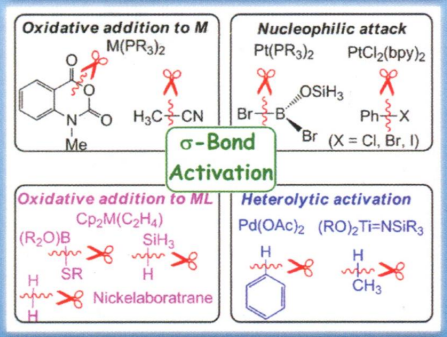

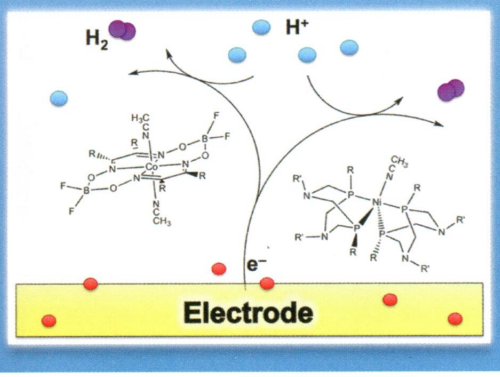

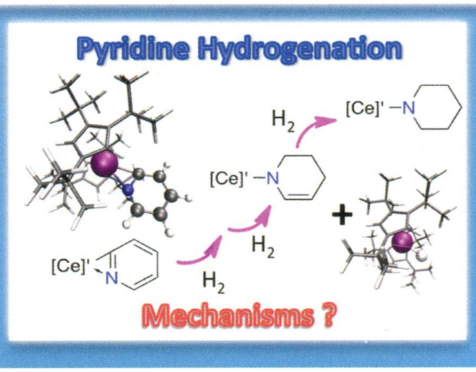

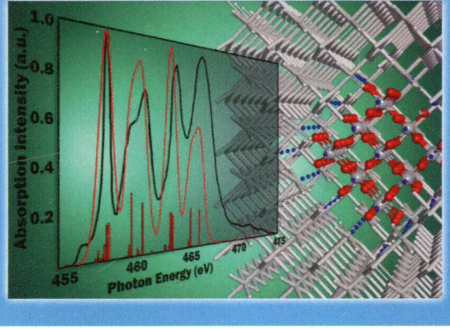

Inorganic Chemistry

JULY 7, 2014
VOLUME 53 ISSUE 13

INOCAJ 53(13) 6357−7070 (2014)
ISSN 0020-1669
Registered in the U.S. Patent and Trademark Office

ON THE COVER: Spectroscopy experimentally defines the electronic structure that underlies the reactivity of inorganic molecules. This issue of *Inorganic Chemistry* presents a Forum on this topic, with contributions from 10 leading researchers illustrated on this cover, that emphasize the application of electronic structure calculations to the spectroscopy, photodynamics, and reactivity of inorganic and bioinorganic molecules and materials.

Forum Articles

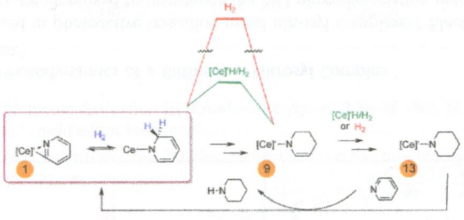

6374 Ⓢ dx.doi.org/10.1021/ic500197v

Restricted Open-Shell Configuration Interaction Cluster Calculations of the L-Edge X-ray Absorption Study of TiO_2 and CaF_2 Solids

Dimitrios Maganas, Serena DeBeer, and Frank Neese*

A DFT/ROCIS cluster study of Ti and Ca L-edge spectra of TiO_2 and CaF_2 solids.

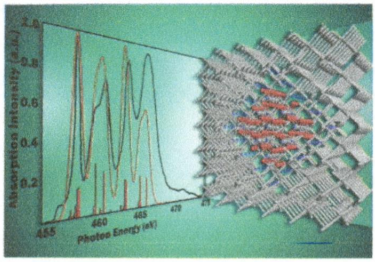

6386 Ⓢ dx.doi.org/10.1021/ic5002557

What Can Density Functional Theory Tell Us about Artificial Catalytic Water Splitting?

Michael G. Mavros, Takashi Tsuchimochi, Tim Kowalczyk, Alexandra McIsaac, Lee-Ping Wang, and Troy Van Voorhis*

This Forum Article reviews the current state-of-the-art computational methods for studying the water-splitting reaction, with particular focus on heterogeneous catalysis. We primarily discuss DFT-based methods for modeling the solvent, explain considerations that must be taken into account when using computation to propose a mechanism, and show how DFT can be used to predict the catalytic activity.

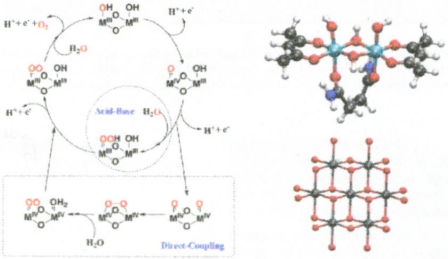

6398 dx.doi.org/10.1021/ic5002573

Characterization of the Bridged Hyponitrite Complex {[Fe(OEP)]$_2$(μ-N_2O_2)}: Reactivity of Hyponitrite Complexes and Biological Relevance

Timothy C. Berto, Nan Xu, Se Ryeon Lee, Anne J. McNeil, E. Ercan Alp, Jiyong Zhao, George B. Richter-Addo,* and Nicolai Lehnert*

The model complex {[Fe(OEP)]$_2$(μ-N_2O_2)} offers a unique opportunity to study the electronic structure and reactivity of hyponitrite-bridged diiron complexes. The ground state of this complex is best described as having two intermediate-spin (S = $^3/_2$) iron centers that are weakly antiferromagnetically coupled. The complex decomposes over time in solution to yield [Fe(OEP)(NO)]. The biological significance of this reaction for nitric oxide reductases is discussed.

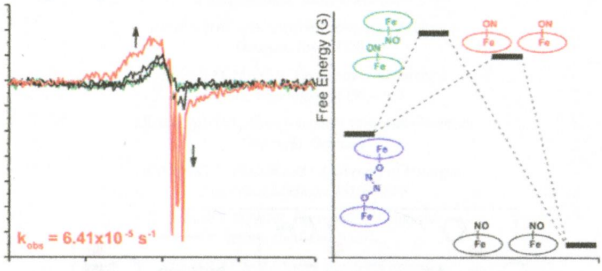

6415 dx.doi.org/10.1021/ic500283y

Theoretical Spectroscopy and Photodynamics of a Ruthenium Nitrosyl Complex

Leon Freitag and Leticia González*

How is nitric oxide (NO) released in photoactive transition-metal nitrosyl complexes? Electronic structure calculations and nonadiabatic molecular dynamics are employed to investigate the NO photodissociation mechanism of [Ru(PaPy$_3$)(NO)]$^{2+}$. Excited states are calculated with time-dependent density functional theory and multiconfigurational CASSCF/CASPT2 spin-corrected methods. Molecular dynamics show that intersystem crossing is ultrafast (10 fs) and that internal conversion takes place in less than 100 fs. Both processes and the competing NO dissociation are accompanied by bending of the NO ligand.

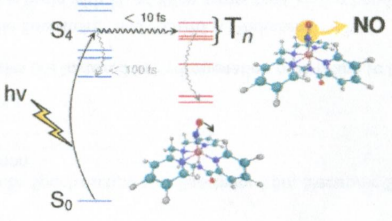

6427 dx.doi.org/10.1021/ic5002896

Proton-Coupled Electron Transfer in Molecular Electrocatalysis: Theoretical Methods and Design Principles

Brian H. Solis and Sharon Hammes-Schiffer*

Molecular electrocatalysis often requires proton-coupled electron transfer processes comprised of sequential or concerted electron and proton transfer steps. Theoretical methods have been used to investigate the thermodynamics and kinetics of these processes and to identify the favorable reaction mechanisms under specified experimental conditions. Theoretical studies have also been used to predict the impact of modifying the ligands, substituents, or metal centers and have guided the design of more effective molecular electrocatalysts.

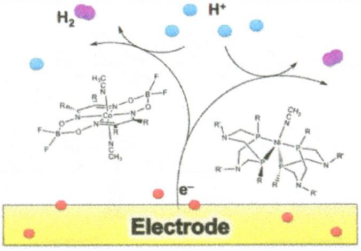

6444 dx.doi.org/10.1021/ic5003429

σ-Bond Activation of Small Molecules and Reactions Catalyzed by Transition-Metal Complexes: Theoretical Understanding of Electronic Processes

Wei Guan, Fareed Bhasha Sayyed, Guixiang Zeng, and Shigeyoshi Sakaki*

σ-Bond activation reactions are classified into such four categories: concerted oxidative addition to a metal center only, stepwise oxidative addition via nucleophilic attack, oxidative addition to M−L (L = neutral ligand), and heterolytic activation by M−X (X = anionic ligand). Experimental examples of these four σ-bond activation reactions are presented, and their characteristic features and electronic processes are discussed based on theoretical studies. Also, a discussion is provided on the important role of the σ-bond activation reaction in the catalytic reaction by a transition-metal complex.

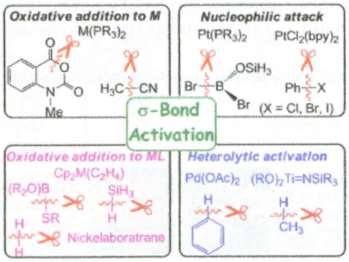

6458 S

dx.doi.org/10.1021/ic500363h

Linking Chemical Electron–Proton Transfer to Proton Pumping in Cytochrome *c* Oxidase: Broken-Symmetry DFT Exploration of Intermediates along the Catalytic Reaction Pathway of the Iron–Copper Dinuclear Complex

Louis Noodleman,* Wen-Ge Han Du, James A. Fee, Andreas W. Götz, and Ross C. Walker

From density functional theory calculations on the dinuclear Fe-a_3–Cu_B complex (DNC) in a type B bacterial cytochrome *c* oxidase, we construct a catalytic reaction wheel diagram for the full redox, O_2 binding, and proton-transfer cycle. A new low-energy pathway is found. Strong shifts in the dipole moment direction/magnitude over the cycle and associated energy differences indicate that the DNC plays a major role not only in the chemical reaction cycle but also in proton pumping.

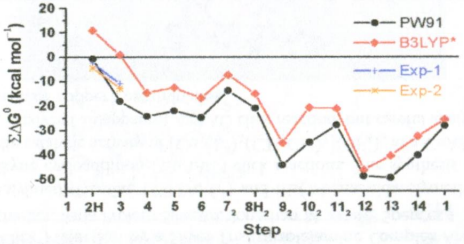

6473 S

dx.doi.org/10.1021/ic500379r

Electronic Structure and Formation of Simple Ferryloxo Complexes: Mechanism of the Fenton Reaction

Alban S. Petit, Robert C. R. Pennifold, and Jeremy N. Harvey*

How do peroxides react with metal ions? The Fenton reaction is perhaps the simplest and most famous example of this broad class of reactions and has been extensively investigated experimentally and computationally. The formation of iron(III) and iron(IV) products has been suggested. In this study, we use very high accuracy explicitly correlated electronic structure theory to pin down the key energetics and conclude that Fe^{III} + OH formation is favored at low pH.

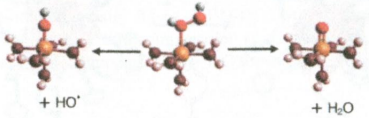

6482

dx.doi.org/10.1021/ic500457q

Reaction Mechanisms of Small-Molecule Activation by Amidoditetrylynes R_2N–EE–NR_2 (E = Si, Ge, Sn)

Markus Hermann, Cameron Jones,* and Gernot Frenking*

Quantum-chemical calculations give insight into the reaction mechanisms of the title reactions.

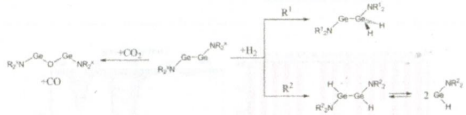

Communications

6491 dx.doi.org/10.1021/ic500732z

Addition of a Second Binding Site Increases the Dynamic Range but Alters the Cellular Localization of a Red Fluorescent Probe for Mobile Zinc

Andrei Loas, Robert J. Radford, and Stephen J. Lippard*

Attachment of a second dipicolylamine binding site greatly increased the dynamic range of ZBR4 and ZR1, the first ditopic members of the resorufin-based family of red fluorescent probes for mobile zinc, and brought about a surprising differentiation in their intracellular localization. Thus, ZBR4 accumulates and detects Zn^{2+} in the mitochondria, while the other ZBR probes and ZR1 primarily target the endoplasmic reticulum.

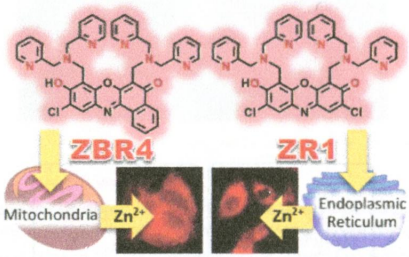

6494 dx.doi.org/10.1021/ic500860t

Lithium Cycling in a Self-Assembled Copper Chloride–Polyether Hybrid Electrode

Adam Jaffe and Hemamala I. Karunadasa*

Incorporation of polyether molecules between copper(II) chloride layers in a hybrid perovskite affords, to the best of our knowledge, the first example of stable Li^+ cycling in a metal chloride electrode. Control experiments demonstrate the importance of the polyether groups and close integration of organic and inorganic components for Li^+ cycling. This work shows that appropriate organic groups can enable Li^+ cycling in inexpensive, nontoxic, metal halide electrodes, which is promising for large-scale applications.

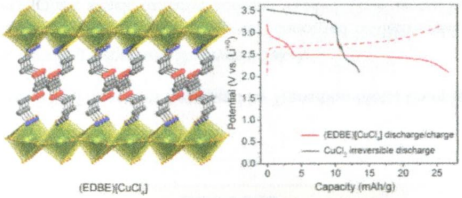

6497 dx.doi.org/10.1021/ic501010s

A Highly Sensitive and Selective Fluorescent Sensor for Detection of Al^{3+} Using a Europium(III) Quinolinecarboxylate

Wentao Xu, Youfu Zhou,* Decai Huang, Mingyi Su, Kun Wang, and Maochun Hong

Eu_2PQC_6 has been developed to detect Al^{3+} by monitoring the quenching in the europium-based emission, with the limit of detection to ~ 32 pM and the quantitative detection range to 150 μM. Eu_2PQC_6 is the first ever example that the europium(III) complex serves as an Al^{3+} fluorescent sensor based on "competition-displacement" mode.

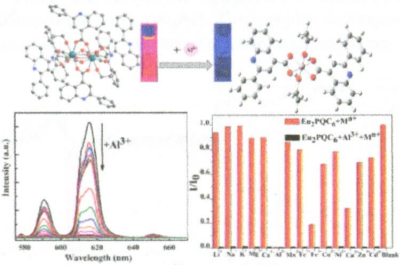

6500 dx.doi.org/10.1021/ic5010819

Structural Basis for Ligand Exchange on $Au_{25}(SR)_{18}$

Thomas W. Ni, Marcus A. Tofanelli, Billy D. Phillips, and Christopher J. Ackerson*

The structural basis of ligand exchange on widely studied $Au_{25}(PET)_{18}$ clusters is established by single-crystal X-ray crystallography.

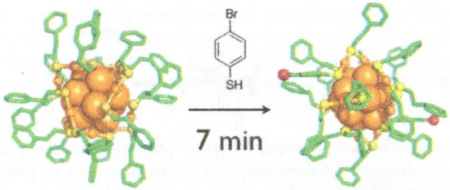

Articles

6503 dx.doi.org/10.1021/ic5008999

Copper and Silver Complexes of Tris(triazole)amine and Tris(benzimidazole)amine Ligands: Evidence that Catalysis of an Azide–Alkyne Cycloaddition ("Click") Reaction by a Silver Tris(triazole)amine Complex Arises from Copper Impurities

Timothy U. Connell, Christine Schieber, Ilaria Proietti Silvestri, Jonathan M. White, Spencer J. Williams,* and Paul S. Donnelly*

Tripodal ligands tris(benzyltriazolylmethyl)amine (TBTA, L^1) and tris(2-benzimidazolylmethyl)amine (L^2) are used to promote Cu^I-catalyzed azide–alkyne cycloaddition (CuAAC) click reactions. The synthesis of silver(I), copper(II), and copper(I) complexes of L^2 and the catalytic activity of $[Cu_3(L^2)_2(CH_3CN)_2](BF_4)_3$ in a CuAAC reaction are reported. An Ag^I complex of L^1, $Ag_2(L^1)_2](BF_4)_2$, catalyzed an apparent AgAAC click reaction, but careful analysis supports the conclusion that catalysis most likely results from trace copper contamination.

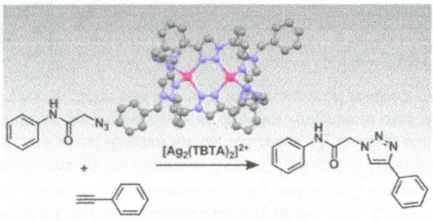

6512 S dx.doi.org/10.1021/ic402574d

A Novel Square-Planar Ni(II) Complex with an Amino—Carboxamido—Dithiolato-Type Ligand as an Active-Site Model of NiSOD

Daisuke Nakane, Yuko Wasada-Tsutsui, Yasuhiro Funahashi, Tsubasa Hatanaka, Tomohiro Ozawa, and Hideki Masuda*

A Ni(II) complex with amino—carboxamido—dithiolato-type coordination is prepared as a model complex of NiSOD. This complex has a quite similar feature to that of the NiSOD active site. The spectroscopic and electrochemical properties of this complex were strongly affected by electrophilicity of solvents. Furthermore, this complex showed similar reactivity with superoxide anion to that of NiSOD. According to the experiments, a reaction mechanism of NiSOD is proposed.

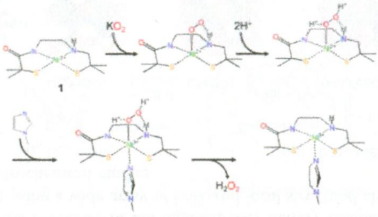

6524 S dx.doi.org/10.1021/ic4028833

Pentanuclear Heterometallic $\{Mn^{III}_2Ln_3\}$ (Ln = Gd, Dy, Tb, Ho) Assemblies in an Open-Book Type Structural Topology: Appearance of Slow Relaxation of Magnetization in the Dy(III) and Ho(III) Analogues

Prasenjit Bag, Amit Chakraborty, Guillaume Rogez,* and Vadapalli Chandrasekhar*

Sequential reaction of a multisite coordination Schiff base ligand (LH_4) with $Mn(ClO_4)_2{\cdot}6H_2O$ and lanthanide(III) nitrate salts in the presence of triethylamine afforded a series of heterometallic pentanuclear dicationic complexes, $[Mn^{III}_2Ln_3(LH)_4(NO_3)(HOCH_3)]ClO_4{\cdot}NO_3\{Ln$ = Gd(**1**),Dy(**2**), Tb(**3**), Ho(**4**)$\}$, possessing an *open-book* type structural topology. Detailed static and dynamic magnetic analysis of all the four compounds revealed single-molecule magnet behavior in the Dy(III) and Ho(III) derivatives.

6534 S dx.doi.org/10.1021/ic403032r

Quantifying Local and Cooperative Components in the Ferroelectric Distortion of $BaTiO_3$: Learning from the Off-Center Motion in the $MnCl_6^{5-}$ Complex Formed in KCl:Mn^+

J. M. García-Lastra,* P. García-Fernández, F. Calle-Vallejo, A. Trueba, J. A. Aramburu, and M. Moreno

The local phase transitions in the KCl:Mn^+ off-center system are investigated through Boltzmann analysis of the vibronic level populations based on ab initio calculations. Decoherence introduced by random strains in the KCl crystal plays a key role in stabilizing low-symmetry geometries. In parallel, the local and cooperative long-range components of ferroelectric distortions in $BaTiO_3$ are analyzed. It is found that the local components in $BaTiO_3$ also have a significant contribution from vibronic coupling, which favors ferroelectricity.

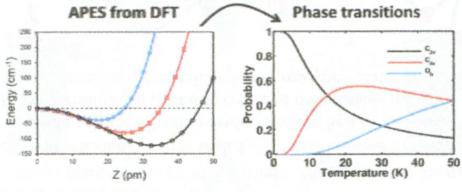

6544 S dx.doi.org/10.1021/ic500051m

Electrocatalytic and Photocatalytic Conversion of CO_2 to Methanol using Ruthenium Complexes with Internal Pyridyl Cocatalysts

David J. Boston, Yeimi M. Franco Pachón, Reynaldo O. Lezna,* N. R. de Tacconi, and Frederick M. MacDonnell*

The ruthenium complex, Ruβ, acts as electro- or photocatalyst for the reduction of CO_2 to deep reduction products such as methanol or formaldehyde. The complex incorporates two functional components, a ruthenium(II) polypyridyl chromophore and a pendant pyridyl function on the lowest-energy acceptor ligand. The latter component is proposed as the essential component for formation of a carbamate radical adduct which is reduced in subsequent electrochemical or photochemical cycles to formate, formaldehyde, or methanol.

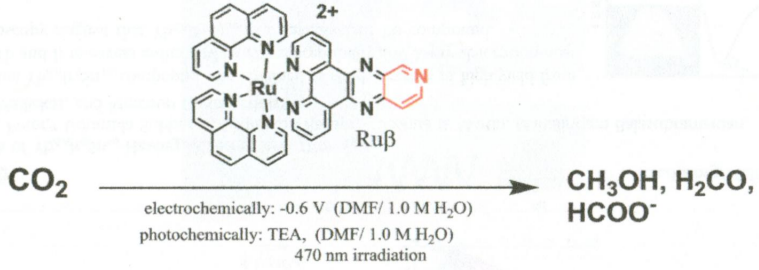

6554 S dx.doi.org/10.1021/ic500085g

Bifunctional Chelates Optimized for Molecular MRI

Erik C. Wiener, Marie-Caline Abadjian, Raghvendra Sengar, Luce Vander Elst, Christoffel Van Niekerk, Douglas B. Grotjahn,* Po Yee Leung, Christie Schulte, Curtis E. Moore, and Arnold L. Rheingold

Multigram preparation of enantiopure bifunctional derivatives of DOTMA for Gd-based contrast agents will enable coupling to targeting systems via click or amide-bond chemistry. The Gd(III)-DOTMA derivative has a shorter water residence time than the Gd(III)-DOTA derivative. Using biotin–avidin complexation to compare constrained systems, the Gd(III)-DOTMA derivative has ~40% higher relaxivity at 37 °C compared to the DOTA analogue, which could increase its sensitivity as an efficient MRI agent.

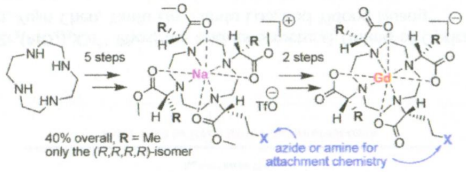

6569 S dx.doi.org/10.1021/ic500137z

Taming the Oxidative Power of SeO_3 in 1,4-Dioxane, Isolation of Two New Isomers of Mixed-Valence Selenium Oxides, and Two Unprecedented Cyclic Esters of Selenic Acid

Lukas Richtera,* Vojtech Jancik,* Diego Martínez-Otero, Ales Pokluda, Zdirad Zak, Jan Taraba, and Jiri Touzin

The kinetic control over the reaction of selenium trioxide with 1,4-dioxane allowed isolation of the first cyclic esters of selenic acid, two different modifications of mixed-valence selenium oxides, namely, Se_4O_{10} and *trans*-Se_3O_7 and the monomeric adduct SeO_3·dioxane. It was also possible to determine the crystal structure of the unstable modification of selenium trioxide $(SeO_3)_3$. These results enrich substantively the chemistry of selenium in the oxidation state VI.

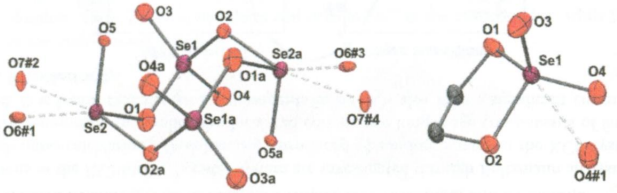

6578 S dx.doi.org/10.1021/ic500162x

First Oxido-Bridged Cubo-Octahedral Hexanuclear Rhenium Clusters

Marta S. Krawczyk,* Monika K. Krawczyk, Miłosz Siczek, and Tadeusz Lis

The new class of single metal clusters with core $Re_6(\mu\text{-}O)_{12}$ adopting cube-octahedral geometry has been obtained in the simple one-pot reaction which can undergo redox reactions maintaining the overall topology.

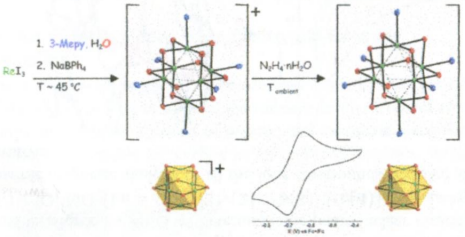

6585 S dx.doi.org/10.1021/ic500169g

Structures of Delithiated and Degraded $LiFeBO_3$, and Their Distinct Changes upon Electrochemical Cycling

Shou-Hang Bo, Kyung-Wan Nam, Olaf J. Borkiewicz, Yan-Yan Hu, Xiao-Qing Yang, Peter J. Chupas, Karena W. Chapman, Lijun Wu, Lihua Zhang, Feng Wang, Clare P. Grey,* and Peter G. Khalifah*

A comprehensive study of the structural evolution of the high capacity battery cathode $LiFeBO_3$ during (de)lithiation and degradation processes was carried out using a wide array of bulk and local structural characterization techniques, both in situ and ex situ, with complementary electrochemical studies.

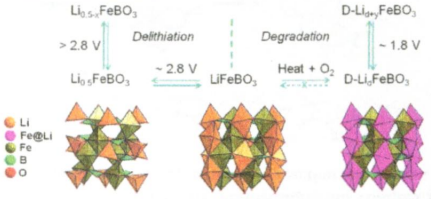

6596 dx.doi.org/10.1021/ic5001733

Synthesis, Characterization, and Photophysical and Electroluminescent Properties of Blue-Emitting Cationic Iridium(III) Complexes Bearing Nonconjugated Ligands

Fuli Zhang,* Dongxin Ma, Lian Duan,* Juan Qiao, Guifang Dong, Liduo Wang, and Yong Qiu

Two series of cationic iridium complexes with nonconjugated ancillary and cyclometalating ligands, respectively, have been prepared. The results showed that the electronic blocker methylene on a nonconjugated ligand plays a significant role in confining the electronic transition dipole of an emitting triplet state mainly around the chromophoric ligands with high LUMO energy levels, and pure blue to deep blue (at 77 K) emission is achieved. Solution-processed blue-green (498 nm) and blue (478 nm) organic light-emitting diodes with maximum current efficiencies of 3.8 and 3.4 cd A^{-1}, respectively, are obtained.

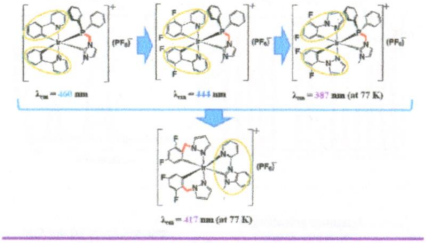

6607 dx.doi.org/10.1021/ic500153u

Novel Garnet-Structure $Ca_2GdZr_2(AlO_4)_3:Ce^{3+}$ Phosphor and Its Structural Tuning of Optical Properties

Xinghong Gong, Jianhua Huang, Yujin Chen, Yanfu Lin, Zundu Luo, and Yidong Huang*

Syntheses, crystal structure, Mulliken bonding population, and photoluminescence properties of $Ca_2GdZr_2(AlO_4)_3:Ce^{3+}$ phosphors are reported. The structural tuning of optical properties of the Ce^{3+}-doped $Ca_2GdZr_2(AlO_4)_3$-based isostructural phosphors are also presented. The emission color of these phosphors could be tuned from blue to green-yellow.

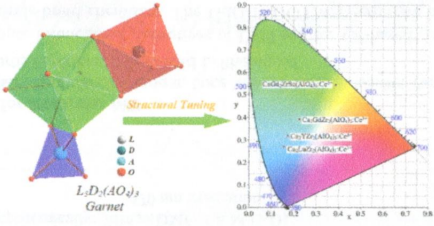

6615 dx.doi.org/10.1021/ic500204t

Flux Growth of $Yb_{6.6}Ir_6Sn_{16}$ Having Mixed-Valent Ytterbium

Sebastian C. Peter,* Udumula Subbarao, Sudhindra Rayaprol, Joshua B. Martin, Mahalingam Balasubramanian, Christos D. Malliakas, and Mercouri G. Kanatzidis*

The tetragonal $Yb_{6.6}Ir_6Sn_{16}$ compound was obtained as single crystals in high yield from reaction of Yb and Ir in excess indium. Magnetic susceptibility and X-ray absorption near edge spectroscopy suggest that $Yb_{6.6}Ir_6Sn_{16}$ is a mixed-valent Yb compound.

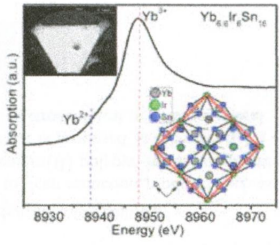

6624 S dx.doi.org/10.1021/ic500232w

Tuning Excited States of Bipyridyl Platinum(II) Chromophores with π-Bonded Catecholate Organometallic Ligands: Synthesis, Structures, TD-DFT Calculations, and Photophysical Properties

Jamal Moussa, Lise-Marie Chamoreau, Alessandra Degli Esposti, Maria Pia Gullo, Andrea Barbieri,* and Hani Amouri*

A series of bipyridyl Pt(II) complexes with π-bonded catecholate (cat) $[(bpy)Pt(L_M)][BF_4]_n$ (**2–5**) (LM= Cp*M(cat), M = Rh, n = 2; M = Ir n = 2; M = Ru, n = 1 and (C_6H_6)Ru(cat), n = 2) is described. The photophysical properties of 2–5 were investigated and showed that all compounds are luminescent at low temperature and in contrast to the parent compound [(bpy)Pt(cat)] (**1**) which is nonluminescent. TDDFT studies are advanced to explain this difference and to highlight the role of the π-bonded catecholate system.

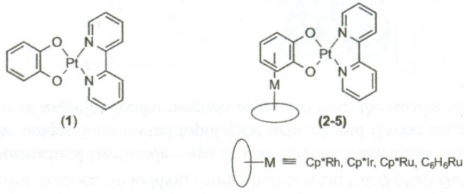

6634 S dx.doi.org/10.1021/ic500258g

A Study on Zr–Ir Multiple Bonding Active for C–H Bond Cleavage

Masataka Oishi, Masato Oshima, and Hiroharu Suzuki*

Zr–Ir hydrido complexes, e.g., **5**, **7**, and **12**, were synthesized and characterized. The hydrocarbyl heterobimetallic complexes displayed the thermolytic C–H activation of aromatic compounds, etc. A Lewis acidic active intermediate generated in the C–H activation, i.e., $(L^1Zr)(Cp^*IrH_2)$ (**III**) was trapped as a Et_3PO-adduct **39b**, which was structurally characterized. Density functional theory (DFT) study showed the unprecedented direct Zr–Ir interactions in **39b** and the relevant intermediates.

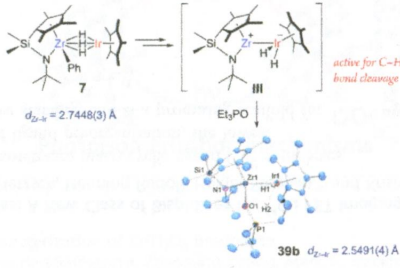

6655 S dx.doi.org/10.1021/ic500313m

Differentially Selective Chemosensor with Fluorescence *Off–On* Responses on Cu^{2+} and Zn^{2+} Ions in Aqueous Media and Applications in Pyrophosphate Sensing, Live Cell Imaging, and Cytotoxicity

Sellamuthu Anbu, Rajendran Ravishankaran, M. Fátima C. Guedes da Silva, Anjali A. Karande, and Armando J. L. Pombeiro*

A benzoyl hydrazone based selective and sensitive dual chemosensor **R** for Cu^{2+} and Zn^{2+} has been synthesized, and their pyrophosphate sensing, bioimaging, and cytotoxic properties have been evaluated.

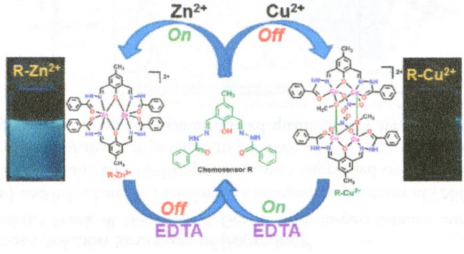

6665 dx.doi.org/10.1021/ic500377w

Reversible Switching of Electronic Ground State in a Pentacoordinated Cu(II) 1D Cationic Polymer and Structural Diversity

Ashok Sasmal, Eugenio Garribba, Corrado Rizzoli, and Samiran Mitra*

Simple deprotonation of carboxylic acid groups causes the transformation of the distorted trigonal bipyramidal into the distorted square pyramidal geometry in Cu(II) complex and structural diversity. The electron-withdrawing effect of the carboxylic acid group weakens the Cu−O and/or Cu−N bonds and induces the flip of the electronic ground state in Cu(II) ion from $d_{x^2-y^2}$ to d_{z^2}.

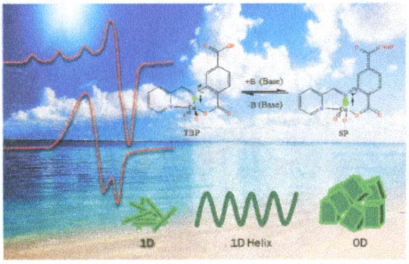

6675 dx.doi.org/10.1021/ic500387u

Insight into the Coordination and the Binding Sites of Cu^{2+} by the Histidyl-6-Tag using Experimental and Computational Tools

Joanna Watly, Eyal Simonovsky, Robert Wieczorek, Nuno Barbosa, Yifat Miller,* and Henryk Kozlowski*

The structures, binding sites and stabilities of the Cu^{2+}-Ac-$(His)_6$-NH_2 complexes have been investigated. The stability of Cu^{2+} species with hexa-histidine tags is exceptionally high and could be derived from strong interactions of the metal cation with two imidazole rings and a very rich landscape of hydrogen bonds. The MD simulations and DFT calculations have shown that Cu^{2+}-$(His)_6$-NH_2 demonstrates polymorphic states with different sets of two bound imidazoles, with a preference for the formation of the α-helix structure.

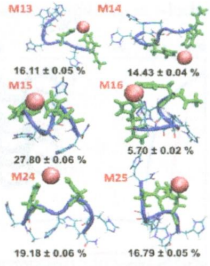

6684 S dx.doi.org/10.1021/ic5004325

Secrets of Solid State and Aqueous Solution Structures of [Ni(tmdta)]$^{2-}$

Roland Meier,* Carlos Platas-Iglesias,* Frank W. Heinemann, Gerald Linti, Jürgen Schulte, and Sunil K. Srivastava

The coexistence of twist-boat (*tb*) and half-chair (*hc*) conformers in aqueous solutions of [Ni(tmdta)]$^{2-}$ has been proved by a combination of vibrational (IR and Raman) and NMR spectroscopies supported by DFT computations. Outstanding matching between theory and experiment made it possible to estimate a *hc*:*tb* ratio of 2:3 for the solutions at room temperature. The kinetics of the skeleton dynamics was estimated quantitatively by temperature-dependent ^{13}C NMR spectroscopic measurements.

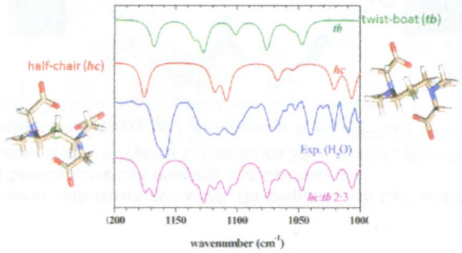

6698 S dx.doi.org/10.1021/ic500476u

Bispidine Dioxotetraaza Macrocycles: A New Class of Bispidines for ^{64}Cu PET Imaging

Peter Comba,* Manja Kubeil, Jens Pietzsch, Henning Rudolf, Holger Stephan,* and Kristof Zarschler

Among the three new bispidine-dioxotetraaza macrocyclic ligand Cu^{II} complexes, that of L^{B} has the highest degree of ligand preorganization, the lowest hydrophilicity and the highest *in vivo* stability, and is a promising scaffold for ^{64}Cu^{II} PET imaging.

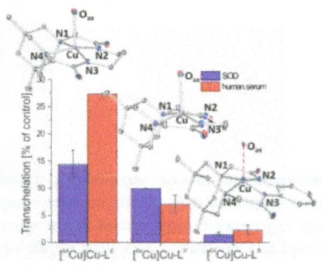

6708 S dx.doi.org/10.1021/ic500490x

Lanthanide–Organic Coordination Frameworks Showing New 5-Connected Network Topology and 3D Ordered Array of Single-Molecular Magnet Behavior in the Dy Case

Min Chen, E. Carolina Sañudo, Erika Jiménez, Shao-Ming Fang, Chun-Sen Liu,* and Miao Du*

Reported herein is a series of isostructural lanthanide–organic coordination frameworks with 5-hydroxyisophthalic acid and 1,10-phenanthroline, showing the unique 5-connected topological network and diverse magnetic behaviors, in which the Dy(III) case is an organized array of single-molecular magnets originated from the smaller ferromagnetic interaction between Dy(III).

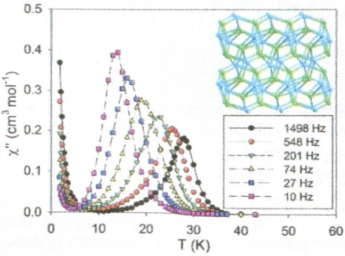

6715 dx.doi.org/10.1021/ic500512e

Kinetics and Mechanism of Styrene Epoxidation by Chlorite: Role of Chlorine Dioxide

Jessica K. Leigh, Jonathan Rajput, and David E. Richardson*

An investigation of the kinetics and mechanism for epoxidation of styrene and *para*-substituted styrenes by chlorite at 25° C in the pH range of 5−6 is described. The proposed quantitative mechanism in water and water/acetonitrile includes seven oxidation states of chlorine (−I, 0, I, II, III, IV, and V) to account for the observed kinetics and product distributions. The central role of ClO_2 and its mechanism of reaction with alkenes are discussed.

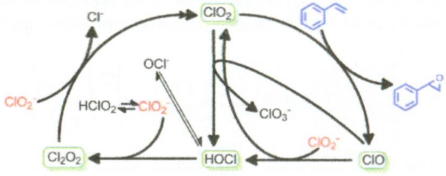

6728 dx.doi.org/10.1021/ic500529b

Stabilization by Si Substitution of the Pseudobinary Compound $Gd_2(Co_{3-x}Si_x)$ with Magnetocaloric Properties around Room Temperature

Sophie Tencé,* Rafael Caballero Flores, Johann Chable, Stéphane Gorsse, Bernard Chevalier, and Etienne Gaudin

We present the discovery of a new solid solution $Gd_2(Co_{3-x}Si_x)$ displaying a ferrimagnetic behavior with a strong composition dependence of the Curie temperature around room temperature.

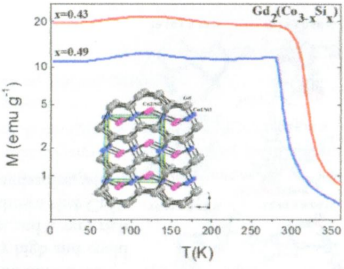

6737 dx.doi.org/10.1021/ic500541h

Hexa- and Trinuclear Organoantimony Oxo Clusters Stabilized by Organosilanols

Pilli V. V. N. Kishore and Viswanathan Baskar*

Syntheses of a series of organoantimony oxo clusters stabilized by organosilanols are reported. Single-crystal X-ray characterization revealed the formation of hexa- and trinuclear metal oxo clusters. Isolation of a mixed-valent organoantimony oxo cluster is also reported herein.

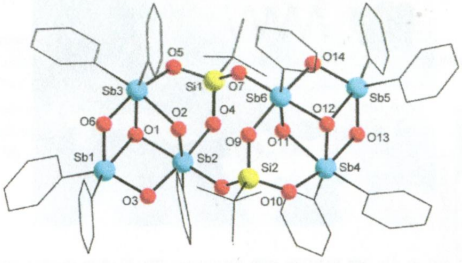

6743 Ⓢ dx.doi.org/10.1021/ic500545y

Synthesis, Luminescence, and Energy-Transfer Properties of β-$Na_2Ca_4(PO_4)_2(SiO_4)$:A (A = Eu^{2+}, Dy^{3+}, Ce^{3+}/Tb^{3+}) Phosphors

Kai Li, Mengmeng Shang, Dongling Geng, Hongzhou Lian, Yang Zhang, Jian Fan, and Jun Lin*

A series of novel β-$Na_2Ca_4(PO_4)_2(SiO_4)$:A (A = Eu^{2+}, Dy^{3+}, Ce^{3+}/Tb^{3+}) phosphors were successfully synthesized by a high-temperature solid-state reaction process.The PL and CL of $Na_2Ca_4(PO_4)_2(SiO_4)$:A (A = Eu^{2+}, Dy^{3+}, Ce^{3+}/Tb^{3+}) were measured to recognize their potential application in wLEDs and FEDs.

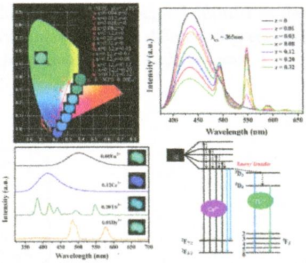

6752 Ⓢ dx.doi.org/10.1021/ic500546q

Unravelling the S → O Linkage Photoisomerization Mechanisms in *cis*- and *trans*-$[Ru(bpy)_2(DMSO)_2]^{2+}$ Using Density Functional Theory

Adrien J. Göttle, Fabienne Alary, Isabelle M. Dixon, Jean-Louis Heully, and Martial Boggio-Pasqua*

The intramolecular S → O linkage photoisomerization of the *cis*- and *trans*-$[Ru(bpy)_2(DMSO)_2]^{2+}$ complexes is investigated using density functional theory. This study reveals that for the *cis* isomer the linkage photoisomerization of the two DMSO ligands occurs sequentially in the lowest triplet excited state and can either be achieved by a one-photon or by a two-photon mechanism. This work especially highlights that both adiabatic and nonadiabatic processes are involved in these mechanisms, and that triplet metal centered states play a crucial role.

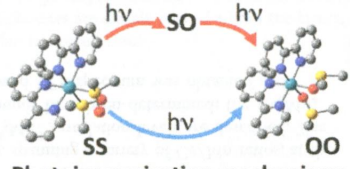

Photoisomerization mechanisms

6761 Ⓢ dx.doi.org/10.1021/ic500563j

Novel Chemical Synthesis and Characterization of $CeTi_2O_6$ Brannerite

Linggen Kong,* Daniel J. Gregg, Inna Karatchevtseva, Zhaoming Zhang, Mark G. Blackford, Simon C. Middleburgh, Gregory R. Lumpkin, and Gerry Triani

Cerium titanate $CeTi_2O_6$ was prepared by a new soft chemistry route in aqueous solution. The chemical reaction took place at the molecular level, which ensured homogeneity of the synthesized powder. The brannerite crystal structure was formed upon calcination at temperatures as low as 800 °C. Sintering at 1350 °C for 50 h led to high crystallinity of the brannerite.

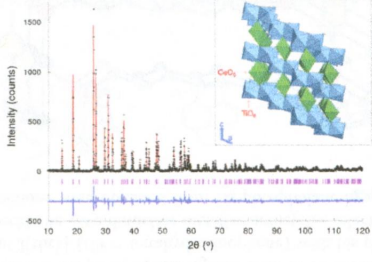

6769 dx.doi.org/10.1021/ic500570u

Investigation of Thorium Salts As Candidate Materials for Direct Observation of the ^{229m}Th Nuclear Transition

Jason K. Ellis, Xiao-Dong Wen, and Richard L. Martin*

Recent efforts to measure the $^{229m}Th \rightarrow {}^{229g}Th$ nuclear transition sparked interest in understanding the electronic structure of wide-gap thorium salts. We show an electronic gap larger than 10 eV for two materials Na_2ThF_6 and ThF_4 suggesting that the internal conversion channel would be suppressed in these materials, making them suitable candidates for measuring this nuclear transition in solid-state devcices.

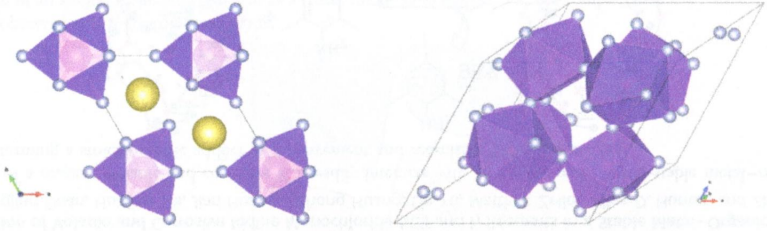

(a) (b)

6775 S dx.doi.org/10.1021/ic5005853

Methylene-Linked Anilide—Bis(aryloxide) Ligands: Lithium, Sodium, Potassium, Chromium(III), and Vanadium(III) Ligation

Yutaka Ishida and Hiroyuki Kawaguchi*

The anilide—bis(aryloxide) proligands H_3[**ONO**], where one anilide and two aryloxide groups are jointed by methylene linkers, were prepared and deprotonated by using alkali metal reagents. The subsequent reactions of the trilithio derivative Li_3[**ONO**] with vanadium(III) and chromium(III) precursors yielded the corresponding mononuclear complexes, in which the [**ONO**] ligand adopts a u-shaped conformation.

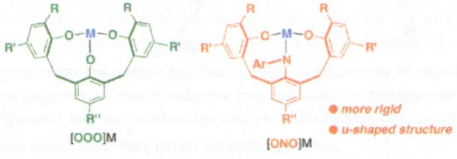

6788 S dx.doi.org/10.1021/ic500592k

Intensive Upconversion Luminescence of Na-Codoped Rare-Earth Oxides with a Novel RE—Na Heterometallic Complex as Precursor

Xiang-Jun Zheng, Ayjamal Ablet, Christie Ng, and Wing-Tak Wong*

A strategy for preparing Na-doped rare-earth oxides with a codoped RE—Na heterometallic complex as precursor was verified to be effective. The obtained codoped oxide Y_2O_3:Yb, Er, Na can give intense red upconversion luminescence upon excitation at 980 nm.

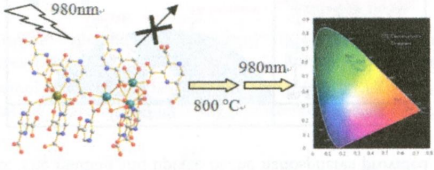

6794 S dx.doi.org/10.1021/ic5006055

Selective Formation of Gold(I) Bis-Phospholane Macrocycles, Polymeric Chains, and Nanotubes

Markus Streitberger, Andy Schmied, and Evamarie Hey-Hawkins*

The coordination behavior of highly flexible bis-phospholane ligands with 5−11 methylene groups in the backbone toward gold(I) is reported. Treatment of [AuCl(tht)] (tht = tetrahydrothiophene) with bis-phospholane ligands having an odd number of methylene groups in the backbone gave dinuclear metallamacrocycles selectively. Polymeric nanotubes and zigzag chains resulting from aurophilic interactions were obtained from bis-phospholane ligands featuring an even number of methylene groups in the backbone.

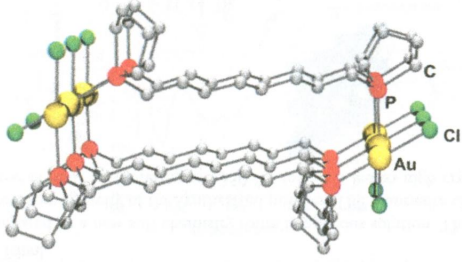

6805 S dx.doi.org/10.1021/ic500617f

Manganese/Cerium Clusters Spanning a Range of Oxidation Levels and $CeMn_8$, Ce_2Mn_4, and Ce_6Mn_4 Nuclearities: Structural, Magnetic, and EPR Properties

Christos Lampropoulos, Annaliese E. Thuijs, Kylie J. Mitchell, Khalil A. Abboud, and George Christou*

The syntheses of three Ce/Mn clusters, spanning a variety of Ce/Mn ratios, at the $Ce^{IV}_6Mn^{III}_2Mn^{IV}_2$, $Ce^{IV}Mn^{III}_8$, and $Ce^{III}_2Mn^{III}_4$ oxidation levels are described. The magnetic properties of all three compounds have been determined; the Ce_6Mn_4 structure is unprecedented, and its X-band EPR spectrum was obtained and simulated.

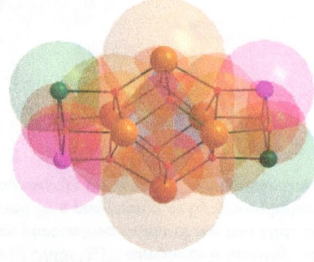

6817 dx.doi.org/10.1021/ic500609g

Synthesis of Luminescent Nanoporous Silica Spheres Functionalized with Folic Acid for Targeting to Cancer Cells
Motohiro Tagaya,* Toshiyuki Ikoma, Zhefeng Xu, and Junzo Tanaka

Luminescent europium(III)-doped nanoporous silica (Eu:NPS) nanospheres were successfully synthesized, and a folate *N*-hydroxysuccinimidyl ester molecule as a targeting ligand for cancer cells was immobilized on the nanospheres. The ordered nanopores were preserved by the immobilization, and the characteristic luminescence from the folic acid functionalized Eu:NPS was detected by fluorescent microscopy. The nanospheres were nontoxic in the cellular proliferation stages and specifically bind to the cancer cells. The binding and uptake of the nanospheres provided an orange luminescence from the cells by the visible-light excitation.

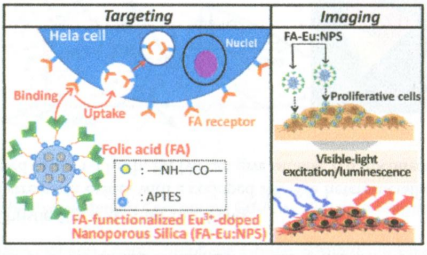

6828 dx.doi.org/10.1021/ic500647j

Role of Aggregation in the Synthesis and Polymerization Activity of SalBinap Indium Alkoxide Complexes
Dinesh C. Aluthge, Ellen X. Yan, Jun Myun Ahn, and Parisa Mehrkhodavandi*

The reactivity of two dinuclear SalBinam indium compounds for the ring-opening polymerization of lactide was investigated. Examination of the polymerization behavior of two complexes and the reaction equilibrium between the two illustrates the importance of aggregation in indium salen complexes compared to their aluminum counterparts.

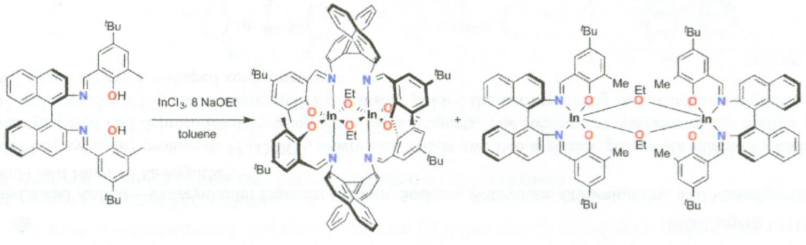

6837 dx.doi.org/10.1021/ic500677t

Immobilization of Volatile and Corrosive Iodine Monochloride (ICl) and I_2 Reagents in a Stable Metal–Organic Framework
Jun He,* Jingjing Duan, Huatian Shi, Jian Huang, Jiahong Huang, Lin Yu, Matthias Zeller, Allen D. Hunter, and Zhengtao Xu*

The taming of a reagent: volatile and corrosive ICl readily interacts with an easy-to-make, water-stable metal–organic framework, forming a stoichiometric adduct as a convenient and recyclable iodinating reagent.

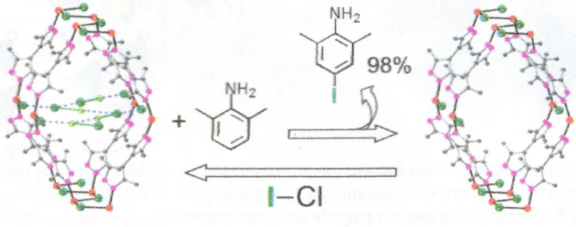

6844 S dx.doi.org/10.1021/ic500688d

Room-Temperature Pressure-Induced Nanostructural $CuInTe_2$ Thermoelectric Material with Low Thermal Conductivity

Atsuko Kosuga,* Kouhei Umekage, Mie Matsuzawa, Yasuhiro Sakamoto, and Ikuya Yamada

A room-temperature high-pressure synthesis is proposed as an alternative way to induce nanoscale structural disorder in the bulk thermoelectric $CuInTe_2$ matrix. This disorder stems from the coexistence of distinct domains with different degrees and geometries of disorder at Cu/In cation sites. The lattice thermal conductivity of high-pressure-treated $CuInTe_2$ was substantially less than that of hot-pressed $CuInTe_2$.

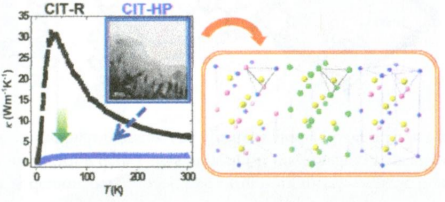

6850 S dx.doi.org/10.1021/ic500689n

Formation of Hexagonal Fullerene Layers from Neutral and Negatively Charged Fullerenes in $\{(Ph_3P)_3Au^+\}_2(C_{60}^{\bullet-})_2(C_{60})\cdot C_6H_4Cl_2$ Containing Gold Cations with the C_{3v} Symmetry

Dmitri V. Konarev,* Salavat S. Khasanov, Akihiro Otsuka, Manabu Ishikawa, Hideki Yamochi, Gunzi Saito, and Rimma N. Lyubovskaya

Fullerene salt $\{(Ph_3P)_3Au^+\}_2(C_{60}^{\bullet-})_2(C_{60})\cdot C_6H_4Cl_2$ containing gold cations with the C_{3v} symmetry was obtained. It contains hexagonal corrugated fullerene layers. The presence of only two cations per three fullerenes allows one to suppose charge disproportionation and the formation of negatively charged and neutral fullerenes. These fullerenes are closely packed within the layers, and the distances between $C_{60}^{\bullet-}$ are essentially longer due to corrugation.

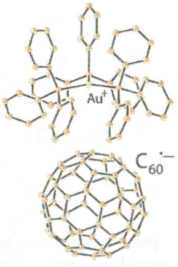

6856 S dx.doi.org/10.1021/ic500697m

Reactivity Profile of a Peri-Substitution-Stabilized Phosphanylidene-Phosphorane: Synthetic, Structural, and Computational Studies

Brian A. Surgenor, Brian A. Chalmers, Kasun S. Athukorala Arachchige, Alexandra M. Z. Slawin, J. Derek Woollins, Michael Bühl, and Petr Kilian*

Peri-substitution-stabilized phosphanylidene-phosphorane ($R_3P{=}PR'$, phospha-Wittig reagent), possessing a sterically accessible two-coordinate phosphorus center, shows diverse coordination chemistry and attains variety of oxidation states in reactions with chalcogens.

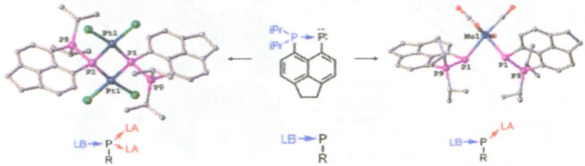

6867 dx.doi.org/10.1021/ic500698v

Three-Coordinate Nickel(II) and Nickel(I) Thiolate Complexes Based on the β-Diketiminate Ligand System

Bettina Horn, Christian Limberg,* Christian Herwig, and Beatrice Braun

Inspired by the threefold S-ligated nickel centers in metalloenzymes, such as CODH or ACS, a bulky nacnac ligand was utilized to synthesize three-coordinate Ni^{II}–SR complexes, which showed reversible reduction waves in cyclovoltammetric investigations. Indeed, the reductions could also be realized chemically employing KC_8 giving dinuclear nickel(I) thiolates. Introduction of an aminoethanethiolate ligand as a closer mimic of cysteinate led to a complex with the nacnac ligand binding in a rarely observed κ^2C,N coordination mode.

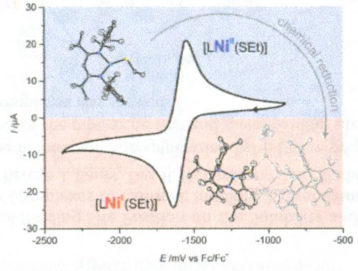

6875 dx.doi.org/10.1021/ic500701a

A Hydrogen-Evolving $Ni(P_2N_2)_2$ Electrocatalyst Covalently Attached to a Glassy Carbon Electrode: Preparation, Characterization, and Catalysis. Comparisons with the Homogeneous Analogue

Atanu K. Das, Mark H. Engelhard, R. Morris Bullock, and John A. S. Roberts*

A hydrogen-evolving homogeneous $Ni(P_2N_2)_2$ electrocatalyst with peripheral ester groups has been covalently attached to a 1,2,3-triazolyllithium-terminated glassy carbon electrode. The surface-confined complex is an electroctalyst for hydrogen evolution, showing the onset of catalytic current at the same potential as that for the soluble parent complex. X-ray photoemission spectra show excellent agreement between the coupled and homogeneous species. Coverage approaches a dense monolayer.

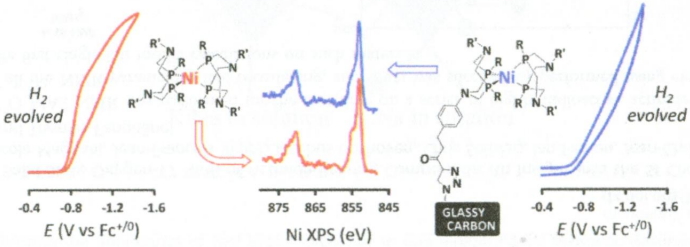

6886 dx.doi.org/10.1021/ic500710t

Polyoxomolybdate-Supported Bismuth Trihalides $[Mo_8O_{26}(BiX_3)_2]^{4-}$ (X = Cl, Br, I): Syntheses and Study of Polymorphism

Sergey A. Adonin,* Eugenia V. Peresypkina, Maxim N. Sokolov, Ilya V. Korolkov, and Vladimir P. Fedin

A family of Bi-containing polyoxomolybdate complexes, $TBA_4[Mo_8O_{26}(BiX_3)_2]$ (X = Cl, Br, I) was obtained by a one-step synthetic procedure. All complexes are characterized by X-ray diffractometry; in all cases, poly- and solvatomorphism was investigated and discussed.

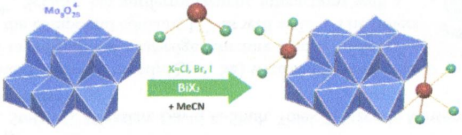

6893 S dx.doi.org/10.1021/ic5007132

Syntheses, Structures, and Physical Properties of $CsRE_2Ag_3Te_5$ (RE = Pr, Nd, Sm, Gd–Er) and $RbRE_2Ag_3Te_5$ (RE = Sm, Gd–Dy)
Chang-Yu Meng,* Hong Chen, and Peng Wang

$ARE_2Ag_3Te_5$ features a 3D mixed covalent and ionic bonding anionic tunnel framework constituted by alternate stacking of the covalently bound $^2_\infty[Ag_3Te_5]$ layer and the ionically bound $^2_\infty[RE_2Te_5]$ layer whose tunnels are filled with A. The sintered sample (containing 1.1–1.7% CsCl impurity) achieves ZTs of 0.02–0.06 at high temperature.

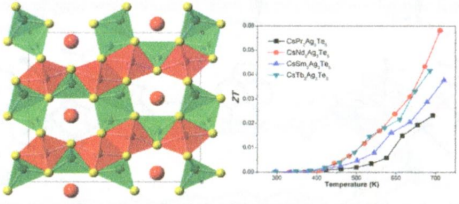

6904 S dx.doi.org/10.1021/ic500709h

New Water Oxidation Chemistry of a Seven-Coordinate Ruthenium Complex with a Tetradentate Polypyridyl Ligand
James T. Muckerman,* Marta Kowalczyk,* Yosra M. Badiei, Dmitry E. Polyansky, Javier J. Concepcion, Ruifa Zong, Randolph P. Thummel, and Etsuko Fujita

Integrated theoretical/experimental studies of water oxidation by the catalyst $[Ru^{II}(dpp)(pic)_2]^{2+}$ ($[\mathbf{Ru}]^{2+}$), with the tetradentate dpp ligand and no water in its primary coordination sphere, reveal unusual behavior in the voltammetry of its first and second oxidations indicating the formation of seven-coordinate complexes $[\mathbf{Ru^{IV}}(O)]^{2+}$ and $[\mathbf{Ru^{V}}(O)]^{3+}$ that incorporate the oxygen atom of a solvent water molecule. The mechanism involves a sequence of seven-coordinate intermediates, and reveals a "new chemistry" associated with this type of molecular catalyst.

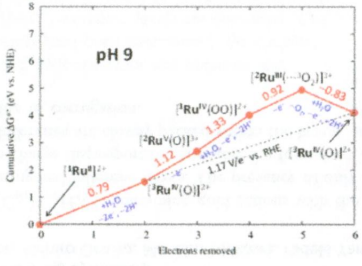

6914 S dx.doi.org/10.1021/ic500722n

Defect Creation by Linker Fragmentation in Metal–Organic Frameworks and Its Effects on Gas Uptake Properties
Gokhan Barin, Vaiva Krungleviciute, Oleksii Gutov, Joseph T. Hupp,* Taner Yildirim,* and Omar K. Farha*

A mixed linker-fragment approach is demonstrated using two promising metal–organic frameworks (MOFs) for gas storage purposes. This strategy is effective for creating defect sites in both MOFs, which in turn allow the tuning of pore volumes and surface areas. The effect of defects on the high-pressure gas uptake is studied over a large temperature and pressure range for different gases.

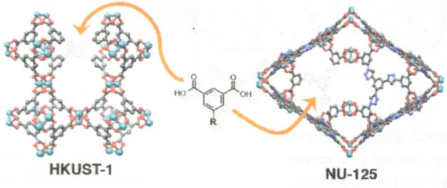

6920 S dx.doi.org/10.1021/ic500721d

Synthesis and Characterization of Eight Compounds of the MU_8Q_{17} Family: ScU_8S_{17}, CoU_8S_{17}, NiU_8S_{17}, TiU_8Se_{17}, VU_8Se_{17}, CrU_8Se_{17}, CoU_8Se_{17}, and NiU_8Se_{17}

Matthew D. Ward, Adel Mesbah, Stefan G. Minasian, David K. Shuh, Tolek Tyliszczak, Minseong Lee, Eun Sang Choi, Sébastien Lebègue, and James A. Ibers*

Eight solid-state MU_8Q_{17} compounds (M = 3d metal; Q = S, Se) were synthesized from the reactions of the elements. X-ray absorption near-edge structure studies of ScU_8S_{17} indicate that it contains Sc^{3+}, so the compound contains U^{3+} as well as U^{4+}. The others charge balance with M^{2+} and U^{4+}. ScU_8S_{17} has antiferromagnetic interactions with a highly reduced effective magnetic moment. Ab initio calculations find the compound to be metallic. The states at the Fermi level originate almost exclusively from U-f states.

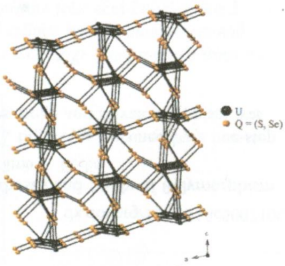

6928 S dx.doi.org/10.1021/ic5007555

High-Resolution Solid-State Oxygen-17 NMR of Actinide-Bearing Compounds: An Insight into the 5f Chemistry

Laura Martel,* Nicola Magnani, Jean-Francois Vigier, Jacobus Boshoven, Chris Selfslag, Ian Farnan, Jean-Christophe Griveau, Joseph Somers, and Thomas Fanghänel

High-resolution ^{17}O MAS NMR was performed for the first time on a series of highly radioactive actinide dioxides. The understanding of all the NMR parameters, line broadening, and shifts was successfully performed using empirical equations combined with the first single-ion model calculations on such materials.

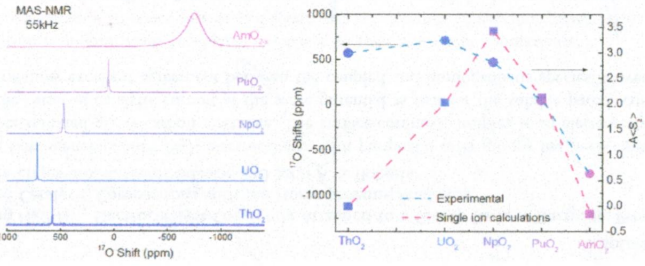

6934 S dx.doi.org/10.1021/ic500825j

Effect of the Piperazine Unit and Metal-Binding Site Position on the Solubility and Anti-Proliferative Activity of Ruthenium(II)- and Osmium(II)- Arene Complexes of Isomeric Indolo[3,2-c]quinoline—Piperazine Hybrids

Lukas K. Filak, Danuta S. Kalinowski,* Theresa J. Bauer, Des R. Richardson,* and Vladimir B. Arion*

Three different structural isomers of the indoloquinoline—piperazine hybrid were prepared *in situ* and isolated as ruthenium- and osmium-arene complexes. The effect of the piperazine unit and metal-binding site position on the aqueous solubility and antiproliferative activity of the metal complexes was studied.

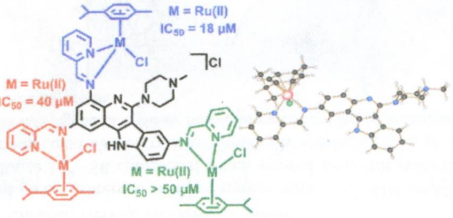

6944 S dx.doi.org/10.1021/ic500833s

The Inverse Trans Influence in a Family of Pentavalent Uranium Complexes

Andrew J. Lewis, Kimberly C. Mullane, Eiko Nakamaru-Ogiso, Patrick J. Carroll, and Eric J. Schelter*

Clear electronic signatures of the inverse trans influence are evident, affording study of this critical determinant of actinide electronic structure across a series of uranium(V) compounds.

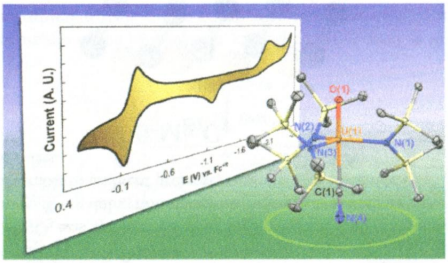

6954 S dx.doi.org/10.1021/ic500861f

"Click" Synthesis of Nona-PEG-branched Triazole Dendrimers and Stabilization of Gold Nanoparticles That Efficiently Catalyze *p*-Nitrophenol Reduction

Na Li, María Echeverría, Sergio Moya, Jaime Ruiz, and Didier Astruc*

Arene-cored, "click" nonabranched PEG dendrimers were synthesized with PEG550 and PEG2000 branches. Following intradendritic Au(III)−triazole complexation, reduction led to AuNPs of various sizes (between 1.8 and 12 nm) controlled by the Au(III)/triazole stoichiometry before $NaBH_4$ reduction. The small mildly stabilized dendrimer-encapsulated AuNPs showed high efficiency in *p*-nitrophenol reduction that also depended on the length of the PEG tethers.

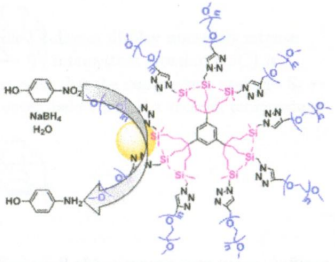

6962 S dx.doi.org/10.1021/ic500891j

Solid-State ^{29}Si NMR and Neutron-Diffraction Studies of $Sr_{0.7}K_{0.3}SiO_{2.85}$ Oxide Ion Conductors

Jungu Xu, Xiaoming Wang, Hui Fu, Craig M. Brown, Xiping Jing, Fuhui Liao, Fengqi Lu, Xiaohui Li, Xiaojun Kuang,* and Mingmei Wu*

In contrast to the average structure with oxygen vacancies stabilized within the isolated 3-fold rings derived from the neutron-diffraction data, solid-state ^{29}Si NMR data provide new insight into the local defect structures of $Sr_{0.7}K_{0.3}SiO_{2.85}$ involving ring-breaking mechanism for corner-sharing to accommodate oxide ion vacancies.

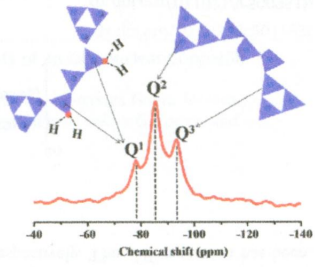

6969 S dx.doi.org/10.1021/ic500877z

Revised Bi/M Layered Oxo-Sulfate (M = Co, Cu): A Structural and Magnetic Study

Minfeng Lü, Marie Colmont, Houria Kabbour, Silviu Colis, and Olivier Mentré*

The combination of oxo-Bi/M mixed slabs with counter oxo-anions main often leads to a series of layered Sillen-related compounds. In the case of SO_4^{2-} anions, only two strongly disordered compounds have been reported for M = Co, Cu, while interesting magnetic topologies emerge in absence of any prior characterization. Our reinvestigation of these systems led to the full structural and magnetic characterization in fully ordered models.

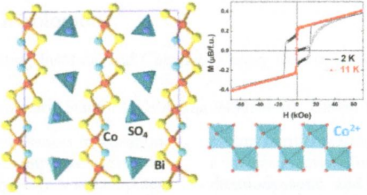

6979 S dx.doi.org/10.1021/ic500922s

How Lewis Acidity of the Cationic Framework Affects $KNaNbOF_5$ Polymorphism

Kelvin B. Chang, Anastasiya Vinokur, Rachelle Ann F. Pinlac, Matthew R. Suchomel, Michael R. Marvel, and Kenneth R. Poeppelmeier*

The polymorphism of $KNaNbOF_5$ crystals formed under mild hydrothermal conditions can be controlled by subtle variations in the K:Na ratio in the reaction mixture. A K:Na ratio of greater than about 1:1 leads to the noncentrosymmetric polymorph, and a lower ratio results in the centrosymmetric polymorph. This synthetic trend correlates with differences in coordination environments of the $[NbOF_5]^{2-}$ anion.

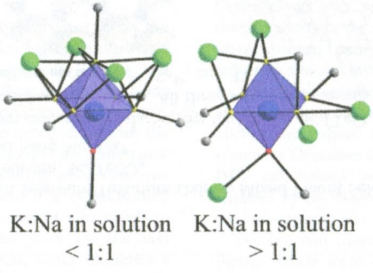

6985 S dx.doi.org/10.1021/ic5008928

Gd(DOTAlaP): Exploring the Boundaries of Fast Water Exchange in Gadolinium-Based Magnetic Resonance Imaging Contrast Agents

Eszter Boros, Shima Karimi, Nathaniel Kenton, Lothar Helm, and Peter Caravan*

Converting one of the acetate groups in the single amino acid chelator DOTAla to methylenephosphonate (DOTAlaP) results in gadolinium(III) complexes with extremely fast water exchange kinetics and/or in equilibrium between monoaquated ($q = 1$) and unaquated ($q = 0$) states. The presence of phosphonate and the very fast water exchange kinetics result in stable complexes with high relaxivity at high magnetic fields, especially when bound to serum albumin.

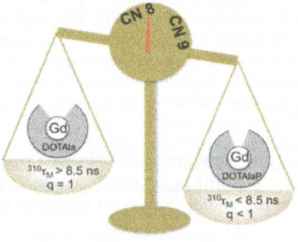

6995 dx.doi.org/10.1021/ic500939t

U–CN versus Ce–NC Coordination in Trivalent Complexes Derived from $M[N(SiMe_3)_2]_3$ (M = Ce, U)

Alexandre Hervé, Yamina Bouzidi, Jean-Claude Berthet,* Lotfi Belkhiri, Pierre Thuéry, Abdou Boucekkine,* and Michel Ephritikhine*

In the series of cyanido-bridged dinuclear compounds and mononuclear mono-, bis-, and tris(cyanide) complexes resulting from addition of cyanide ions to $[M\{N(SiMe_3)_2\}_3]$ (M = Ce, U), the bis(cyanide) complexes revealed distinct coordination modes of the CN group, through the C or N atom to the U or Ce metal center, respectively. This differentiation has been analyzed using relativistic density functional theory (DFT) calculations.

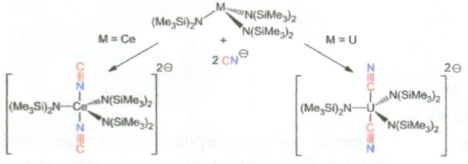

7014 dx.doi.org/10.1021/ic500951b

Exploration of Chemically Cross-Linked Metal–Organic Frameworks

C. A. Allen and S. M. Cohen*

A series of geometrically constrained cross-linked benzene dicarboxylic acid (bdc) derivatives have been synthesized and incorporated into the canonical isoreticular metal–organic framework (IRMOF) lattice. These rationally designed ligands are preorganized for coordinating the Zn_4O secondary building unit (SBU) and creating the desired cubic architecture. These ligands demonstrate a high level of rational design that can lead to new crystal engineering opportunities with metal–organic frameworks.

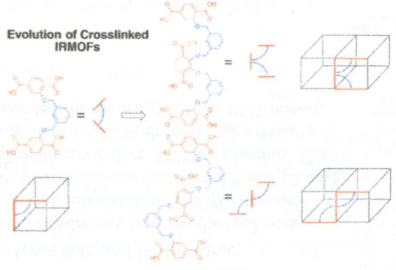

7020 dx.doi.org/10.1021/ic500960d

Synthesis of β-Mg_2C_3: A Monoclinic High-Pressure Polymorph of Magnesium Sesquicarbide

Timothy A. Strobel,* Oleksandr O. Kurakevych, Duck Young Kim, Yann Le Godec, Wilson Crichton, Jérémy Guignard, Nicolas Guignot, George D. Cody, and Artem R. Oganov

A new monoclinic polymorph of Mg_2C_3 was synthesized using high-pressure, high-temperature methods. The crystal structure was solved by combining synchrotron X-ray diffraction data with accurate evolutionary algorithm crystal structure predictions. The new compound, which is recoverable to ambient pressure, contains rare allylenide (C_3^{4-}) anions that are all approximately aligned along the crystallographic *c*-axis.

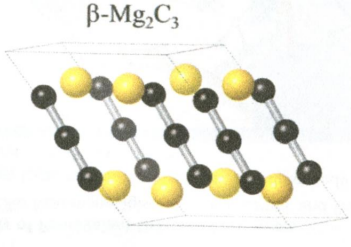

7028 dx.doi.org/10.1021/ic501001r

Structural Diversity and Physical Properties of Paramagnetic Molecular Conductors Based on Bis(ethylenedithio) tetrathiafulvalene (BEDT-TTF) and the Tris(chloranilato)ferrate(III) Complex

Matteo Atzori, Flavia Pop, Pascale Auban-Senzier, Carlos J. Gómez-García, Enric Canadell, Flavia Artizzu, Angela Serpe, Paola Deplano, Narcis Avarvari,* and Maria Laura Mercuri*

This Paper reports on structural diversity and physical properties of three new magnetic molecular conductors formulated as $[BEDT\text{-}TTF]_3[Fe(Cl_2An)_3]\cdot 3CH_2Cl_2\cdot H_2O$ (**1**), δ-$[BEDT\text{-}TTF]_5[Fe(Cl_2An)_3]\cdot 4H_2O$ (**2**), and α'''-$[BEDT\text{-}TTF]_{18}[Fe(Cl_2An)_3]_3\cdot 3CH_2Cl_2\cdot 6H_2O$ (**3**), which are among the first examples of radical cation salts containing the tris(chloranilato)-ferrate(III) complex.

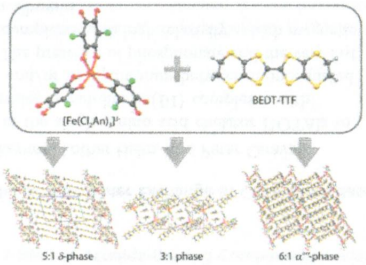

7040 dx.doi.org/10.1021/ic501009c

Rich Structural Chemistry in Scandium Selenium/Tellurium Oxides: Mixed-Valent Selenite–Selenates, $Sc_2(SeO_3)_2(SeO_4)$ and $Sc_2(TeO_3)(SeO_3)(SeO_4)$, and Ternary Tellurite, $Sc_2(TeO_3)_3$

Seung Yoon Song, Dong Woo Lee, and Kang Min Ok*

Three new scandium selenium/tellurium oxides materials, $Sc_2(SeO_3)_2(SeO_4)$, $Sc_2(TeO_3)(SeO_3)(SeO_4)$, and $Sc_2(TeO_3)_3$, have been prepared by hydrothermal and solid-state reactions. All three reported materials exhibit three-dimensional framework structures composed of asymmetric cations such as Sc^{3+}, Se^{4+}, and Te^{4+}.

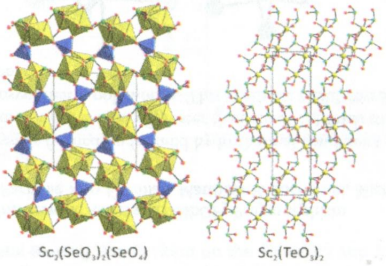

7047 Ⓢ dx.doi.org/10.1021/ic501103c

Synthesis and Reactivity Studies of a Tin(II) Corrole Complex

Lin Yun, Hugo Vazquez-Lima, Huayi Fang, Zhengmin Yao, Georg Geisberger, Christian Dietl, Abhik Ghosh,* Penelope J. Brothers,* and Xuefeng Fu*

This Article reports the synthesis of a novel four-coordinate, divalent tin corrole complex $[(TPFC)Sn^{II}]^-$ (**2a**) by facile reduction of $(TPFC)Sn^{IV}Cl$ (**1a**) using $NaBH_4$. The anion **2a** showed highly efficient reactivity toward alkenes and alkyl halides via a nucleophilic addition pathway leading to the quantitative formation of alkyl stannyl corrole compounds. DFT calculations confirmed the divalent nature of the tin center in **2a**, and an NBO analysis showed about 99.99% Sn lone pair character.

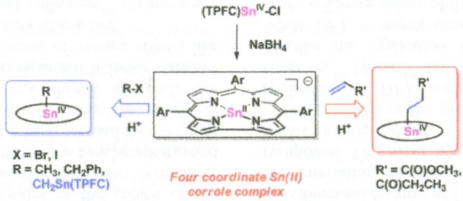

7055 Ⓢ dx.doi.org/10.1021/ic501115k

Fluorescence in Rhoda- and Iridacyclopentadienes Neglecting the Spin–Orbit Coupling of the Heavy Atom: The Ligand Dominates

Andreas Steffen,* Karine Costuas,* Abdou Boucekkine, Marie-Hélène Thibault, Andrew Beeby, Andrei S. Batsanov, Azzam Charaf-Eddin, Denis Jacquemin, Jean-François Halet,* and Todd B. Marder*

Despite the presence of heavy atoms 2,5-bis(arylethynyl)rhoda- and iridacyclopenta-2,4-dienes display unusually intense fluorescence from the S_1 excited state and no phosphorescence from T_1. The $S_1 \rightarrow T_1$ intersystem crossing (ISC) is remarkably slow, with a rate constant of $10^8\ s^{-1}$. Emission lifetime measurements suggest that the compounds undergo $S_1 \rightarrow T_1$ interconversion mainly via a thermally activated ISC channel above 233 K. However, below 233 K a second, temperature-independent ISC process via spin–orbit coupling occurs.

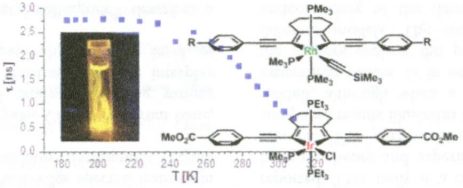

Additions and Corrections

7070 dx.doi.org/10.1021/ic501183f

Correction to Antitumoral, Antihypertensive, Antimicrobial, and Antioxidant Effects of an Octanuclear Copper(II)-Telmisartan Complex with an Hydrophobic Nanometer Hole

María S. Islas, Juan J. Martínez Medina, Libertad L. López Tévez, Teófilo Rojo, Luis Lezama, Mercedes Griera Merino, Laura Calleros, María A. Cortes, Manuel Rodriguez Puyol, Gustavo A. Echeverría, Oscar E. Piro, Evelina G. Ferrer, and Patricia A. M. Williams*

Ⓢ Supporting Information available via online article